GEANT simulation for the Longitudinal Polarimeter

Wolfgang Lorenzon, Sergey Rudnitsky, Andreas Most

February 18, 1997

1 Introduction

To determine the polarization of the electron beam we have to measure an asymmetry in the energy deposited in the calorimeter by Compton photons that originate from scattering of the left and right circularly polarized laser light off the electron beam. Backscattered Compton photons have different cross sections for two polarization states of the laser light. This difference in the cross sections translates into different distributions of photons on the front face of the detector for the two laser light helicities. If there is any sensitivity of the detector to the position at which the photon hits the detector it will have an impact on the value of the measured asymmetry and hence the value of the electron beam polarization. This sensitivity of the detector to the position of the incident beam on the front face of the detector is called acceptance function and has been studied using experimental data and Monte-Carlo simulations. Since the acceptance function together with the linearity of the detector completely determines the response of the detector the agreement or disagreement between experimental and Monte-Carlo results will confirm or deny the validity to the results obtained using Monte-Carlo simulations. In the following sections we present results of the Monte-Carlo simulation and discuss their bearing on the total systematic error of the Polarimeter.

1.1 Acceptance function

As mentioned above one of the main properties of the calorimeter is its acceptance function, which can be obtained by scanning a beam of fixed energy accross the face of the detector. As we do so we can record energy deposition in each of the crystals by charged particles as well as the amount of light collected on the PMT's for each position of the incident beam. One of the main questions that had to be answered, even before doing full scale Monte-Carlo analysis of the properties of the detector, was whether we can utilize an energy acceptance function, which

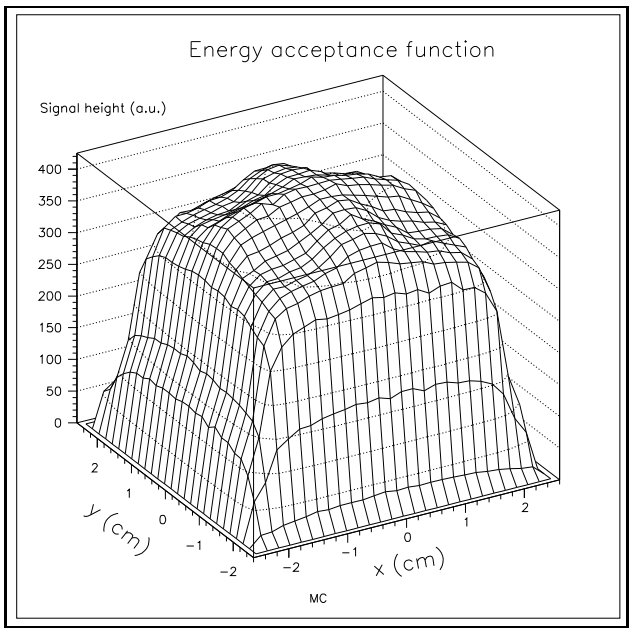

Figure 1: Energy acceptance function

is just the energy deposited in the crystals as a function of the incident beam position, instead of the acceptance function based on the response of the PMT's to Cherenkov light. If it were possible, then we could reduce running time for Monte-Carlo simulations since it would not be necessary to generate Cherenkov photons in the simulation and then track them through the detector. We could also become less dependent on the parametrizations used to generate Cherenkov photons. As it turns out, even though two acceptance functions are not drastically different there are still some differences in shape, that are very characteristic of our detector and therefore can not be neglected. As we can see in Fig.1, the height of the signal is the largest at the center of the detector and gradually becomes smaller as we move towards the the edges of the crystals. If we compare this acceptance function with the Cherenkov light acceptance function given in Fig.2, than we can see that the latter lacks depressions in front of the PMT's, which gives it a more rounded shape. This effect is due to a weaker shower development closer to the edges of the crystals being compensated by one of the PMT's situated directly in front of the shower. Given this difference in shapes it is reasonable to use Cherenkov light acceptance function, which gives more precise results at the expense of somewhat bigger CPU usages for our Monte-Carlo study.

Taking into account the importance of the acceptance function, it is also instructive to look at the acceptance function for a single crystal, presented in Fig.3. As we can see the signal height almost vanishes to zero as the position of the incident beam crosses the boundary between this and any of the adjacent

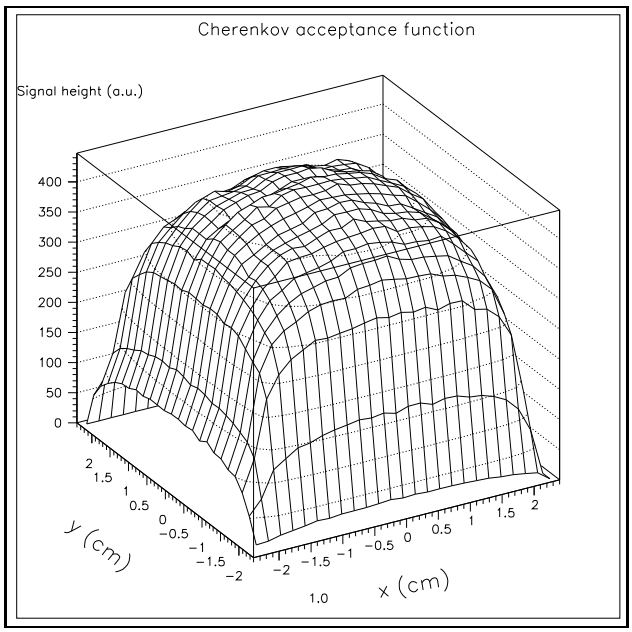

Figure 2: Cherenkov light acceptance function.

crystals. This can be partially attributed to the fact that we have optical isolation between crystals, which does not allow Cherenkov light to pass from one crystal into another, and therefore the light collection on the PMT is entirely determined by the shape of the shower (Moliere radius 2.38 cm) and its position with respect to the PMT.

Before we can use any acceptance function as a representation of the response of the calorimeter we should check its dependence on the energy of the incident beam. If it changes shape as we scan the energy of the incident beam through the possible range of energies for backscattered Compton photons or if the detector is non-linear, we can no longer use a single acceptance function as a basis for further Monte-Carlo simulations. Since the energy of Compton photons lies within 0-13.6 GeV range, we can generate two acceptance functions that correspond to the incident beam energies of 1 and 13 GeV and compare them. If there are no significant changes in the shape as we go from one energy to another, than we can safely assume that the accepance function remains the same over the entire energy range. The result of this comparison is presented in Fig.4. The ratio of the two acceptance functions has been renormalized to one at the center of the four NBW crystal array, so that only the difference in shape would be left over. As we can see the ratio remains approximately one across the entire surface, except right outside the edges of the crystals. This can be accounted for by noticing that the absolute signal height in this region is extremely small as compared to one at the center of the calorimeter and therefore large statistical fluctuations are possible

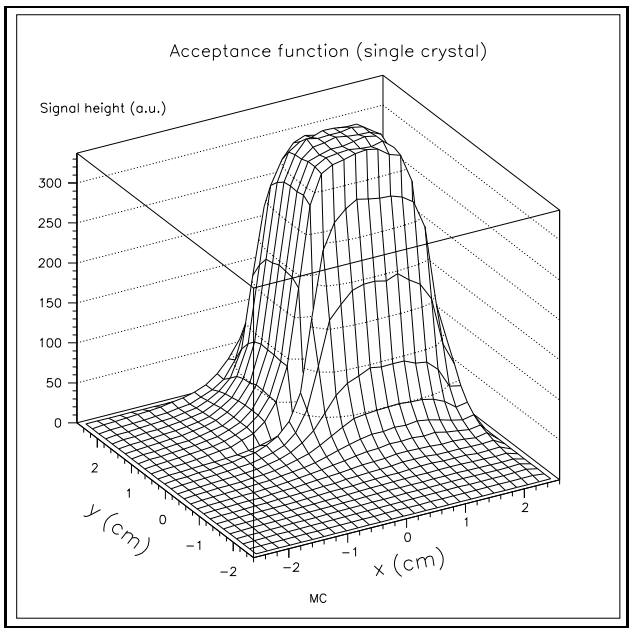

Figure 3: Energy acceptance function for a single crystal.

as well as by the possible non-linearity of the calorimeter when the incident beam position is situated outside of the NBW crystals. The ripple on the remaining part of the surface is due to statistical fluctuations. All the remaining deviations of the ratio of the acceptance functions from one are well withing 5% and, as it will be shown later, are insignificant. Therefore, Monte-Carlo acceptance functions pass the "shape test".

1.2 Linearity of the calorimeter.

Next, we have to address the issue of the linearity of the calorimeter. The linearity plot is presented in Fig.5. The detector response was taken at energies of 1,3,6,9 and 13 GeV. As it turns out the detector is linear within 1% as can be seen in Fig.6. This has less than 0.5% effect on the value of asymmetry and we assume that the calorimeter passes the "linearity test".

Since the acceptance function passed the "linearity" and "shape" tests, we can use a single function to represent response of the calorimeter at all energies in the Monte-Carlo simulation.

The remaining issue, before we proceed with using a Monte-Carlo derived acceptance function for further investigations is whether it reproduces the experimental one. The ratio of the Monte-Carlo and experimental acceptance functions, renormalized to one at the center of the detector, is presented in Fig.7.

As we can see the two acceptance functions agree to within 10% across the

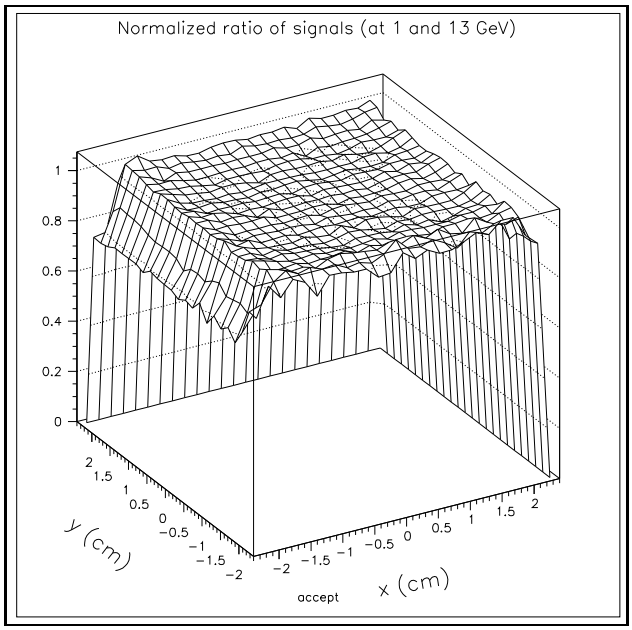

Figure 4: Comparison of acceptance functions at 1 and 13 GeV.

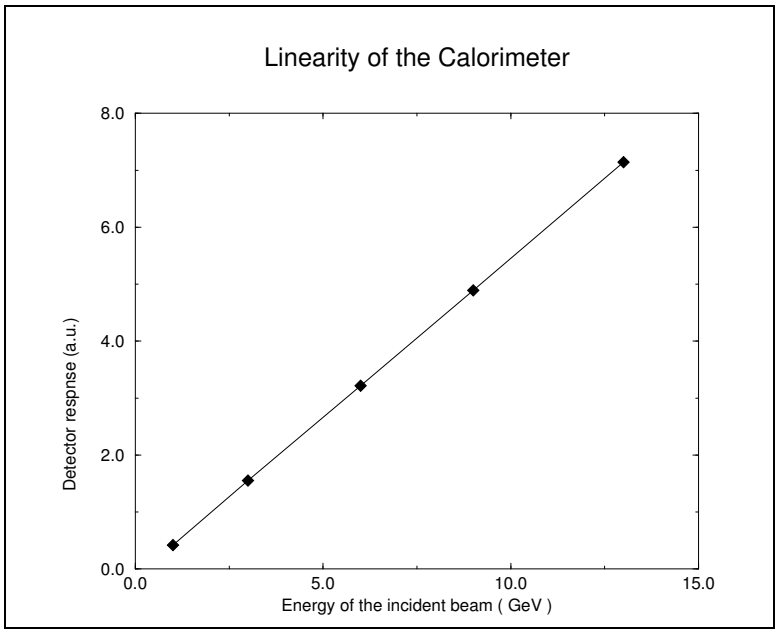

Figure 5: Linearity of the calorimeter.

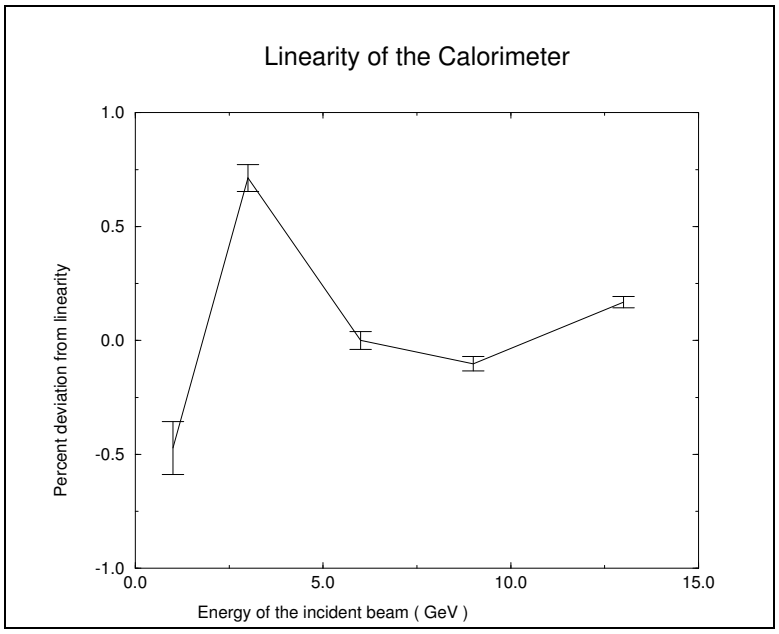

Figure 6: Deviation from the linearity of the calorimeter.

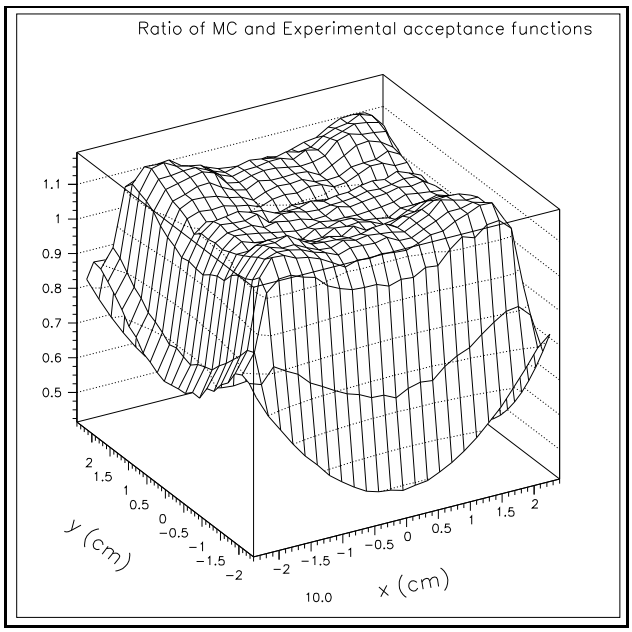

Figure 7: Comparison of Monte-Carlo and experimental acceptance functions.

entire surface of the calorimeter, except in the region outside of the NBW crystals, which can be attributed to the reasons as large deviations of the renormalized ratio from one in Fig.4. The 10% agreement over the remaining portion of the surface of the calorimeter has a negligible impact on the value of the asymmetry. We can also notice that the largest deviations are at the edges of the crystals where Compton photons that hit the calorimeter have the lowest energy and the cross section asymmetry is the smallest. Therefore, they contribute insignificantly to the total energy asymmetry for two opposite helicity states of the laser light.

1.3 Energy asymmetry.

Now we deal with the most important point, namely energy asymmetry for two helicity states of the laser light for 100% longitudinally polarized electron beam. The result of the analytical calculation based on the known cross sections that does not take into account neither variations of the acceptance function over the surface of the calorimeter nor the finite size of the detector, which leads to the low energy Compton photons missing the detector, predicts 18.37% asymmetry. However, due to the above mentioned effects energy asymmetry changes to 18.41%. This corresponds to 0.2% change in the value of the asymmetry and since the measured polarization value of the electron beam linearly depends on the energy asymmetry, it is a very important quantity to determine. Moreover, if the calorimeter is offset with respect to the geometrical center of the Compton distribution, then the value of the asymmetry can also change, since the acceptance function is not constant over the surface of the calorimeter. The result of the Monte-Carlo simulation is presented in Fig.8.

As we can see the energy asymmetry turns out to be a weak function of the position of Compton distribution on the front face of the detector. There is no need to worry about this position dependence in doing on-line or off-line data analysis, its effect can be characterized at worst by an extra 0.5% contribution towards the total systematic error as it is shown in Fig.9.

1.4 Gain shifts.

Another important issue is the stability of the polarization measurement with respect to the gain drifts of one of the PMT's. An effect of the 10% gain drift of one of the PMT's on the total acceptance function is presented in Fig.10, which can be compared with the acceptance function given in Fig.1 that corresponds to a case when all of the four PMT's are matched.

A value of the asymmetry function that corresponds to an absolute gain drift of one of the PMT's within 20% is plotted in Fig.11. The gains of all the other channels have been fixed. From Fig.11 we conclude that a 20% change in the gain leads to no change in the asymmetry value.

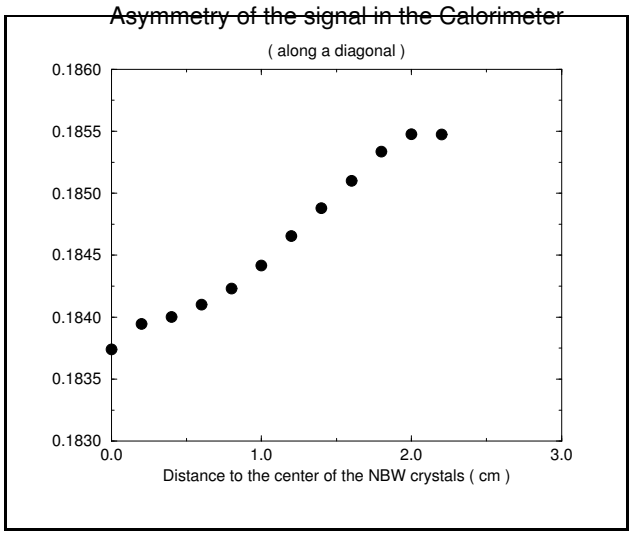

Figure 8: Energy asymmetry for two opposite helicity states of the laser light.

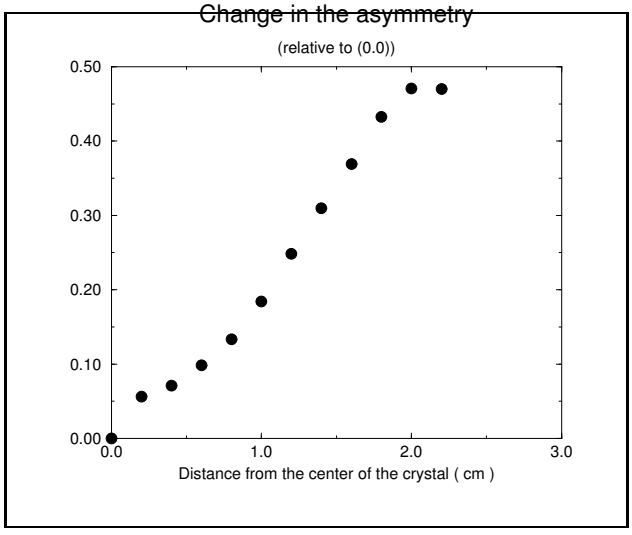

Figure 9: Relative change in the energy asymmetry.

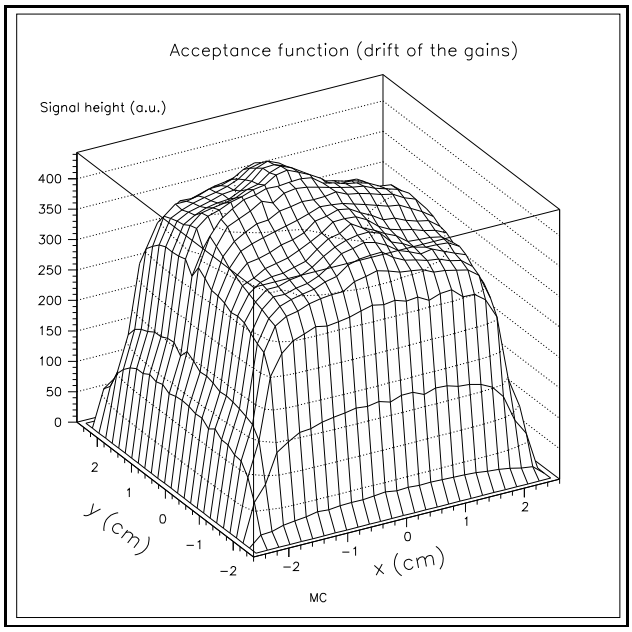

Figure 10: Energy acceptance function, (one of the PMT gains drifted by 10%).

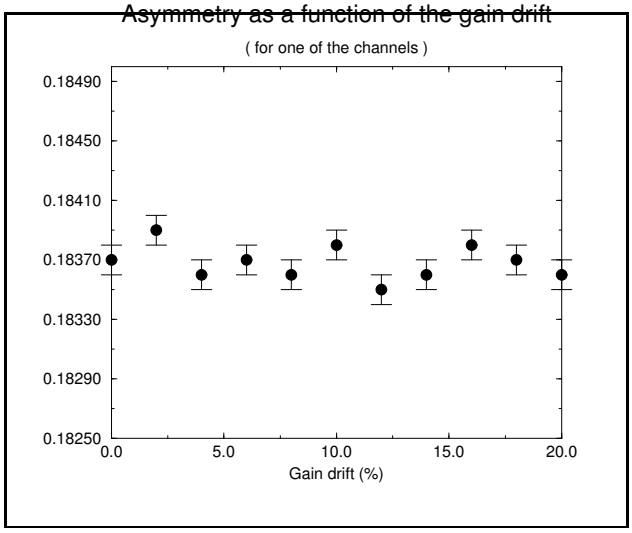

Figure 11: Change in the energy asymmetry as a function of a gain drift.

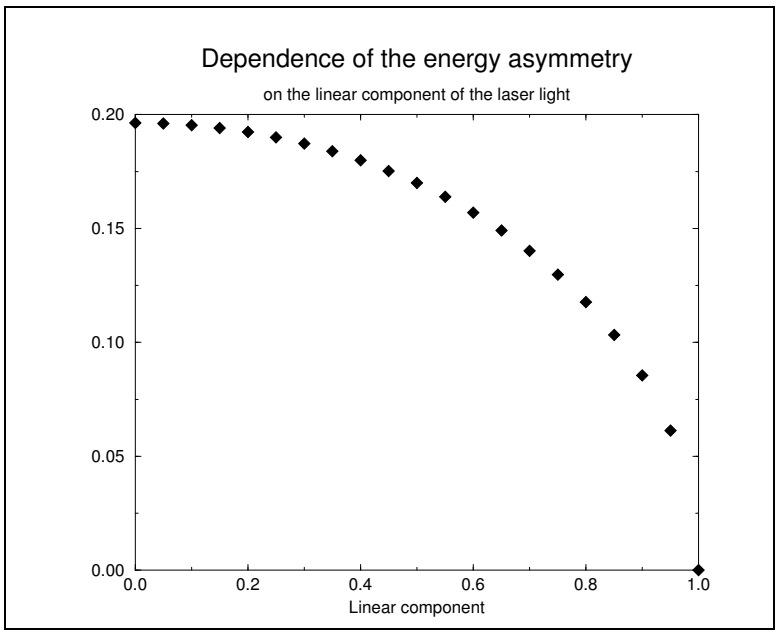

Figure 12: Effect of the linear component on the energy asymmetry.

1.5 Linear component of the laser light.

It is also interesting to study the dependence of the energy asymmetry on the linear component of the laser light. This dependence obtained as a result of the Monte-Carlo simulation is presented in Fig.12. As it is expected the energy asymmetry decreases as the linear component of the laser light increases. The important point is that as long as the linear component stays below 15% change in the energy asymmetry remains negligible, see Fig.13.

1.6 Energy resolution.

Based on the Monte-Carlo data we can also calculate energy resolution of the calorimeter. It turns out to be $15.4\%/sqrt(E)$ (see Fig.14), which is in a good agreement with the test beam results that gave us $18.0\%/sqrt(E)$ energy resolution. The difference between the two results is expected to have come from the energy resolution of the test beam itself.

1.7 Eta to Y transformation.

The last subject that had been touched by our Monte-Carlo study is the so- called η-to-y transformation, which is given in Fig.15, parameters of the fit are given below:

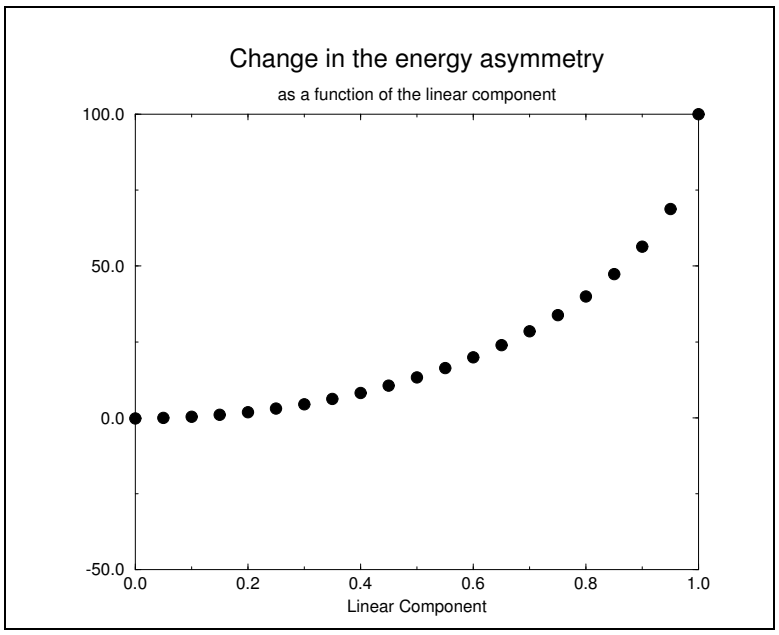

Figure 13: Relative change in the energy asymmetry as a function of linear component.

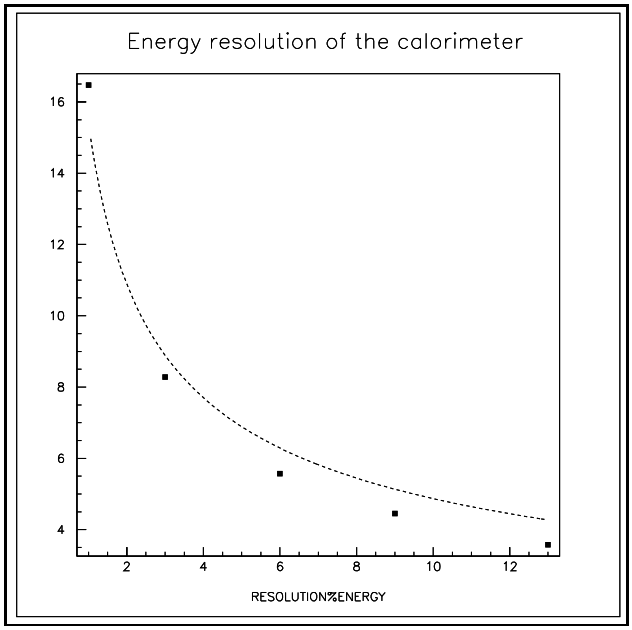

Figure 14: Energy resolution of the calorimeter.

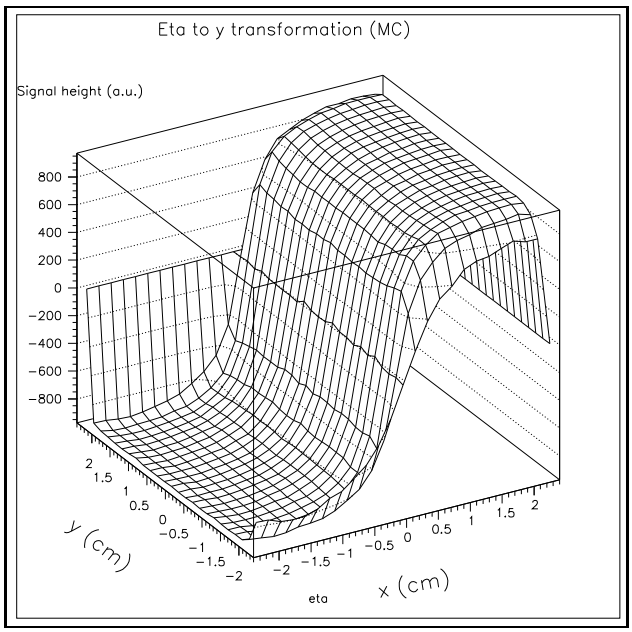

Figure 15: η to y transformation.

$$\eta = 1.0 - 0.2 * exp(-(\mid Y \mid)/29.45) - 0.8 * exp(-(\mid Y \mid)/4.25)$$

2 Appendix

Here we give a short description of interactive commands used in Geant simulation of the Longitudinal polarimeter.

1) dtree - displays the geometrical tree in a hierarchical representation of the structure of the detector, based on the mother-daughter relationship among the various volumes composing it. If you run it then you will see what is presented in Fig.16.

2) Clicking the left mouse button on the specified volume or else choosing interactive "dspec" command for that volume will display the geometrical specifications for the volume. For example, MBOX is a mother box in which the detector is positioned, CALO is the calorimeter itself and NBW is nbw crystal. Corresponding figures are presented in Fig.17, Fig.18, Fig.19.

3) dcut mbox 1 1 10 10 .4 .4 - displays a side view of the calorimeter.

4) dcut mbox 2 1 10 10 .4 .4 - displays a top view of the calorimeter.

5) dcut mbox 3 -10 5 10 1 1 - displays a front view of the calorimeter.

The result of the option 3) can be seen in the Fig.20.

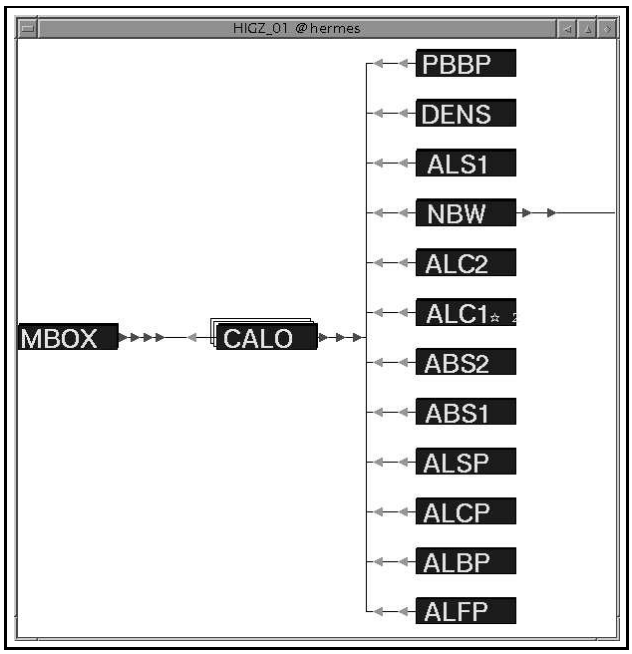

Figure 16: Hierarchical layout of the detector components.

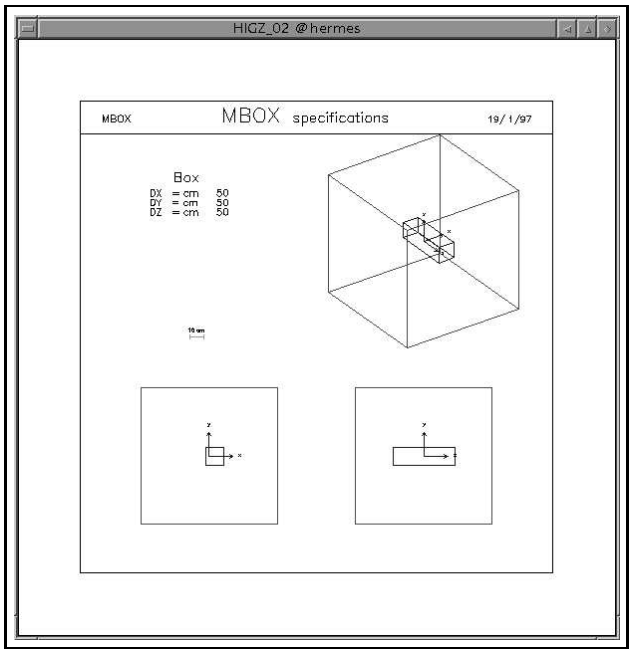

Figure 17: Mother box

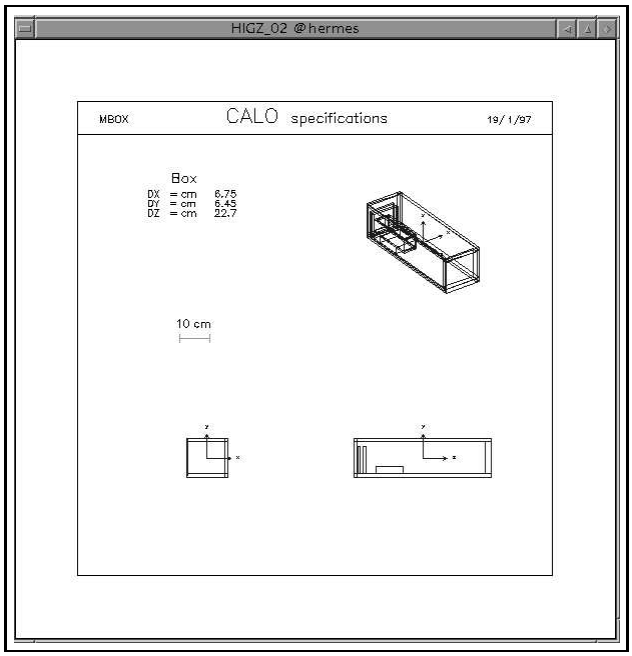

Figure 18: Calorimeter

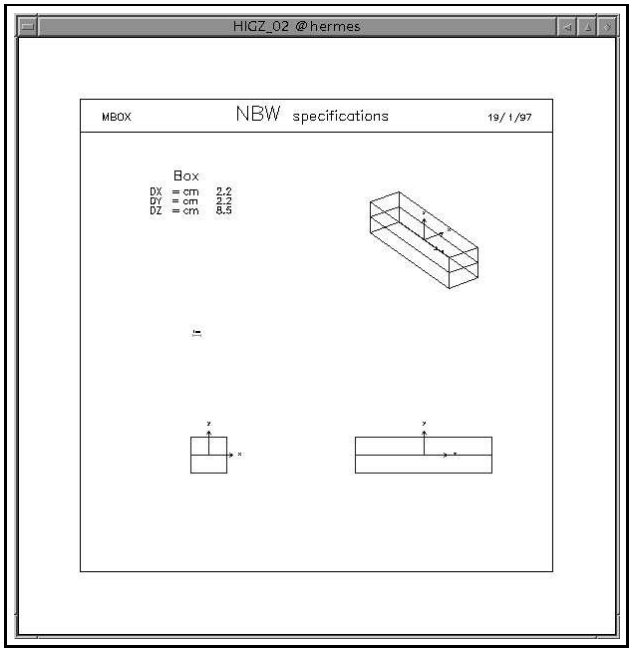

Figure 19: NBW crystals

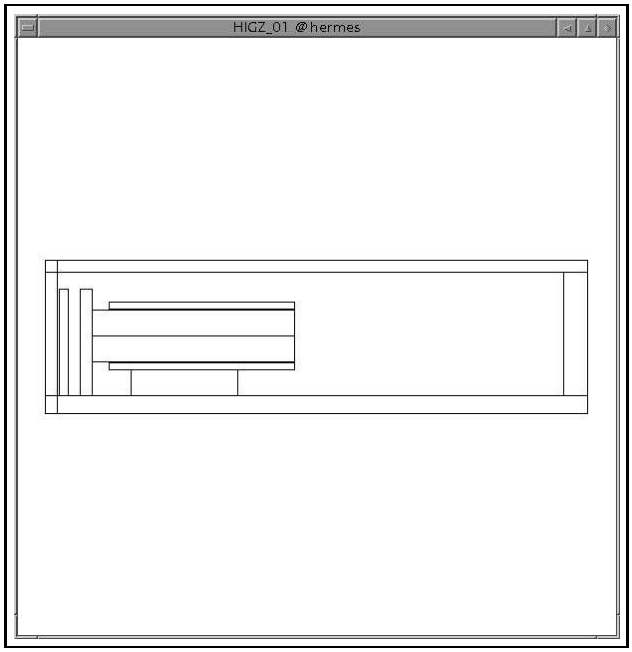

Figure 20: Cross-section of the detector

6) deb on - initializes debugging option.
7) swit 2 4 - initializes track plotting.
8) swit 2 0 - turns off track plotting.
9) trig - triggers one event.

If you set the debug option on then it would be possible to see all of the events tracked through the detector media, as in the Fig.21.

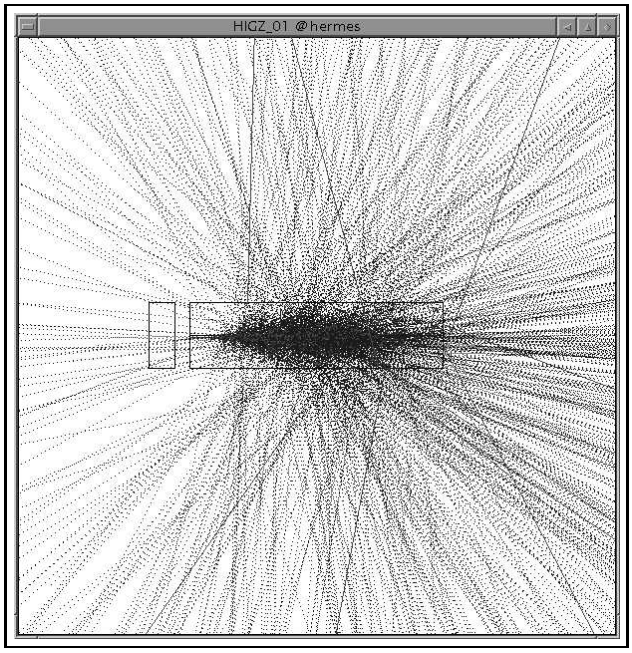

Figure 21: Tracks in the detector